Dynamic Pore Filtering for Keypoint Detection applied to Newborn Authentication

Rubisley de Paula Lemes[1], Maurício Pamplona Segundo[2], Olga R. P. Bellon[1], and Luciano Silva[1]

[1]IMAGO Research Group, Universidade Federal do Paraná, Brazil.
[2]Department of Computer Science, Universidade Federal da Bahia, Brazil.
rubisley@inf.ufpr.br, mauricio@dcc.ufba.br, olga@inf.ufpr.br, luciano@inf.ufpr.br

***Abstract*—We present a novel method for newborn authentication that matches keypoints in different interdigital regions from palmprints or footprints. Then, the method hierarchically combines the scores for authentication. We also present a novel pore detector for keypoint extraction, named Dynamic Pore Filtering (DPF), that does not rely on expensive processing techniques and adapts itself to different sizes and shapes of pores. We evaluated our pore detector using four different datasets. The obtained results of the DPF when using newborn dermatoglyphic patterns (2400ppi) are comparable to the state-of-the-art results for adult fingerprint images with 1200ppi. For authentication, we used four datasets acquired by two different sensors, achieving true acceptance rates of 91.53% and 93.72% for palmprints and footprints, respectively, with a false acceptance rate of 0%. We also compared our results to our previous approach on newborn identification, and we considerably outperformed its results, increasing the true acceptance rate from 71% to 98%.**

***Keywords*—Newborn recognition; dermatoglyphic patterns; pore detection.**

I. Introduction

Nowadays, nearly 131 million children are born every year in the entire world[1]. Among them, there are many cases of baby swaps, child kidnapping and illegal adoption due to the lack of proper newborn identification methods. Within this context, biometrics are emerging as a solution since they can be used in maternity wards or airports to solve these problems [1], [2], [3], [4], [5].

In this work, we present a novel method for newborn authentication based on the matching of keypoints extracted from palmprints or footprints, also called dermatoglyphic patterns. None of the above mentioned works has used keypoints for newborn recognition purposes. One reason, may be the difficulty in capturing suitable images that allow extracting and describing keypoints. Instead, they used other biometrics, such as face [2], [5], ear [4] or friction ridges in dermatoglyphic patterns [3]. However, these biometrics change after birth, thus not meeting the immutability criterion.

To extract keypoints, we have used a well-known corner detector [6] and we have also designed a pore detection algorithm. Recently, pores have been explored in adult fingerprint recognition [7], [8]. However, current methods for pore extraction rely on processing techniques such as ridge reconstruction and estimation of orientation and frequency, which may be both expensive and not suitable on poor quality images (*e.g.* newborn dermatoglyphic patterns). Therefore, as our first contribution, we have designed a new pore detection method, named Dynamic Pore Filtering (DPF). This method does not rely on expensive processing steps and adapts itself to different sizes and shapes of pores. Some examples of pores with different sizes and shapes are shown in Figure 1.

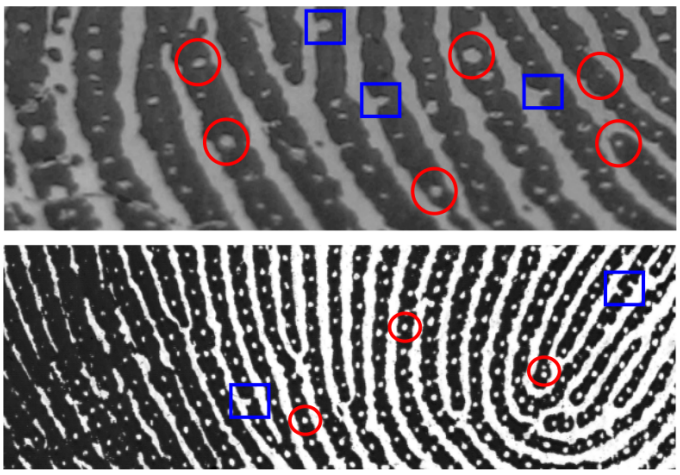

Fig. 1. Pores in dermatoglyphic patterns: circles show closed pores; squares show open pores.

Our second contribution is the use of keypoints (*i.e.* corners and pores) for newborn authentication using dermatoglyphic patterns. The matching is individually performed for each interdigital region of palmprints and footprints based on the spatial relation between keypoints. Then, the matching scores are hierarchically evaluated for authentication.

Keypoint-based biometric recognition solutions are being widely used in the literature [9], [10]. In our problem, we are interested in extracting keypoints for recognizing individuals using dermatoglyphic digital images. Within this context, we have used a well-known corner detection approach, called Features from Accelerated Segment Test (FAST) [6]. The FAST detector is a corner-based keypoint extraction method, which may be used for many vision problems, such as object tracking and recognition [11]. Corners are commonly used as keypoints, and FAST is considered one the most efficient corner detectors in the literature [6]. Also, we developed a pore detection approach, DPF, which was specifically designed for newborn dermatoglyphic patterns.

This paper is organized as follows. In Section II we

[1]http://data.worldbank.org/indicator/SP.DYN.CBRT.IN/countries

describe the proposed method for pore detection (DPF). Section III presents the hierarchical matching approach. Our experimental evaluation is presented in Section IV. Finally, our final remarks are discussed in Section V, followed by the references.

II. Dynamic Pore Filtering

The proposed method for pore detection is divided into the following stages: (A) Region of Interest (ROI) extraction and image equalization; (B) global binarization threshold estimation; (C) pore size estimation; (D) pore classification; and (E) pore location estimation.

A. ROI extraction and image equalization

This stage is performed as in [1]. To do so, first we rectify the image orientation and remove finger or toe regions from palmprints or footprints, respectively, as in [12]. Then, the Contrast Limited Adaptive Histogram Equalization (CLAHE) [13] is employed to normalize the image appearance.

B. Global binarization threshold estimation

In this stage, a global binarization threshold T_G is estimated by Otsu's method [14]. This method is able to automatically compute the threshold for an image with two distinct pixel classes, which is the case of dermatoglyphic patterns (*i.e.* ridges and valleys). After this stage, only pixels with value above T_G are going to be evaluated, since pores are always bright regions.

C. Pore size estimation

For each pixel with value above T_G, we search for the closest neighbor with value under T_G in four directions: up, down, left and right. There is a maximum search distance to find these neighbors, which was empirically defined as 20 pixels in this work. This threshold is based on the analysis of the size of pores in multiple images from different subjects and acquisition devices. If more than one direction reaches this maximum value, the current pixel is discarded since it is considered a valley point.

Figure 2 illustrates five examples of this process, labeled with the letters A, B, C, D and E. Candidates A and B are closed pores, C and D are valley points, and E is an open pore. As may be seen, candidate C reaches the maximum search distance in up and down directions, so it is discarded in the next stages. Closed pores always reach a neighbor in all directions, and open pores may have one direction without a neighbor.

A global pore radius r_G is then computed using Equation 1:

$$r_G = \frac{1}{4|P|} \sum_{p \in P} (d^p_{up} + d^p_{down} + d^p_{left} + d^p_{right}) \qquad (1)$$

where P is the set of pixels with value above T_G and at least three known neighbors, and d^p_θ is the distance of the current pixel p to its neighbor in the direction θ.

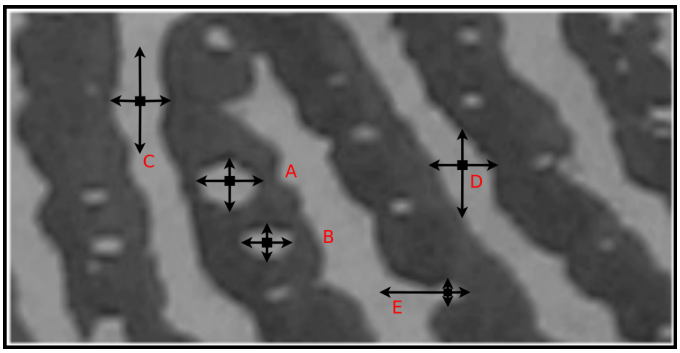

Fig. 2. Pore size estimation examples.

D. Pore classification

For each pixel $p \in P$, a local binarization threshold T_L is defined as the average of the pixels in a $6r_G \times 6r_G$ mask centered on p (*i.e.* since $2r_G$ is the average width of pores and valleys, the size $6r_G$ ensures that the mask will contain at least one valley and one ridge in it). Also, a local pore radius r_L is computed using Equation 2:

$$r_L = \frac{1}{4|P'|} \sum_{p \in P'} (d^p_{up} + d^p_{down} + d^p_{left} + d^p_{right}) \qquad (2)$$

where P' is the set of pixels in P that are also inside the mask defined above. The values for T_L and r_L can be efficiently computed using integral images [15].

We then analyze the pixels in a circle with radius r_L around the current pixel p to determine if it is a pore. Figure 3 shows six examples of these circles, labeled with the letters A, B, C, D, E and F. As may be seen, the radius value adapts to the size of the pores, labeled as B, D and F. The pixels in the circle are classified as valley if above T_L (shown in white in Figure 3), and as ridge otherwise (shown in black in Figure 3).

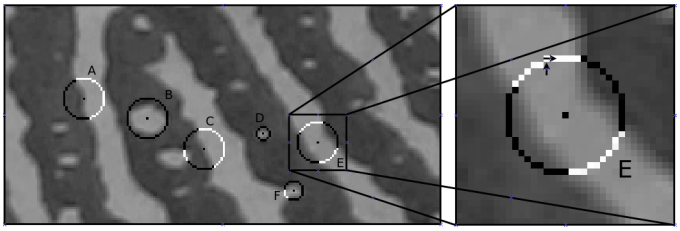

Fig. 3. Circles with size r_L around pore candidates.

Then, each pixel is classified as a pore if it satisfies the following three conditions:

- The number of valley pixels must be smaller than 40% of the number of pixels in the circle (*i.e.* pores are surrounded by ridge pixels, so the number of ridge pixels in the bounding circle must be high, as may be observed in candidates B, D and F in Figure 3). This threshold was empirically defined based on the analysis of the number of pixels in the circle in multiple images from different subjects and acquisition devices;

- Only one transition between contiguous pixels of same type (valley or ridge) is allowed (*i.e.* closed pores do not have any transition, as may be observed in candidates B and D in Figure 3; open pores have one transition, as may be observed in candidate F in Figure 3);
- The average value of the pixels in the circle is below T_L (*i.e.* pixels in the bounding circle are mostly ridge pixels, so their average value is low).

Figure 4 shows some results after the pore classification stage for images with different resolution and dermatoglyphic patterns. Also, the variation in the size of the pores is very high, but, as may be observed, the presented method is able to detect pores across all these variations. Most of the false positives are caused by small saliences in the ridges that look like open pores, although bifurcations are also a problem. These problems are highlighted in Figure 4(b).

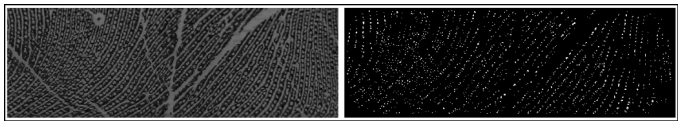

(a) Newborn palmprint – 2400ppi

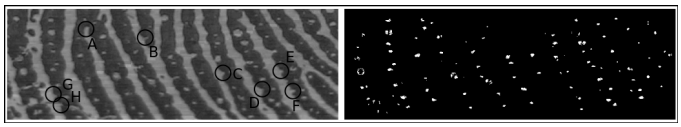

(b) Adult fingerprint – 2400ppi

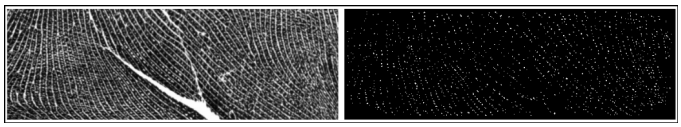

(c) Newborn palmprint – 1000ppi

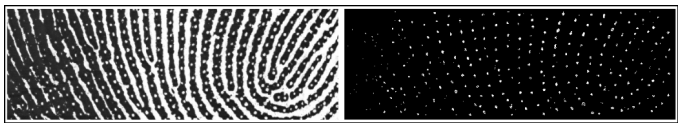

(d) Adult palprint – 1000ppi

Fig. 4. Pore classification results: white pixels in images of the right column were classified as pore after the application of the initial four stages of the proposed method on the images of the left column.

E. Pore location estimation

In this final stage, all connected pore pixels are transformed into a single point by computing their center of mass. Figure 5 shows an example of the keypoints extracted from a palmprint image using FAST and DPF.

III. Matching

Once we extracted a set of keypoints $P_A = \{p_1^A, p_2^A, \ldots, p_N^A\}$ from an image A, where $p_i^A = \{x_i^A, y_i^A\}$ and N is the number of keypoints, a local descriptor d_i^A is computed for every point in P_A. We applied the DAISY approach [16] to compute these descriptors because it outperformed other state-of-the-art descriptors, such as SIFT [17] and SURF [18], in our experiments. This descriptor

(a) FAST

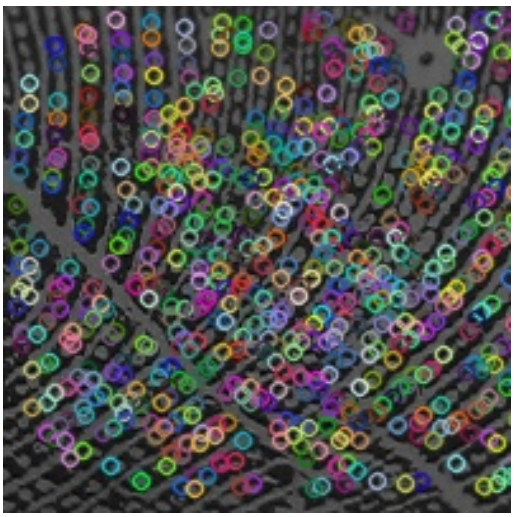

(b) DPF

Fig. 5. Keypoint detection using (a) FAST and (b) DPF.

was originally developed for stereo matching, so it is not robust to large variations in orientation and scale, which is not a problem in our images.

To match two images A and B, first we need to establish point correspondences in the sets P_A and P_B. To this end, a correspondence c_{ij} matching points p_i^A e p_j^B must satisfy Equations 3 and 4:

$$\min_k \|d_i^A - d_k^B\|, k = j \tag{3}$$

$$\min_k \|d_k^A - d_j^B\|, k = i \tag{4}$$

We used kd-trees [19] to speed up the search for the set of correspondences C, which is then used to compute the matching score s_{AB} as in Equation 5:

$$s_{AB} = \frac{1}{|C|} \sum_{\forall c_{ij} \in C} \sum_{\forall c_{kl} \in C} \frac{1}{1 + |\|p_i^A - p_k^A\| - \|p_j^B - p_l^B\||} \tag{5}$$

This score is high if A and B belong to the same person (genuine matching), because the difference in the distance between two points in P_A and the distance between their corresponding points in B is very small if the correspondences are correct. For images from different subjects (impostor matching), this difference is usually large because all correspondences are incorrect, then the score value is low.

To decide if A and B belong to the same person, we verify if s_{AB} is above a threshold t. If t is high, the chance of a pair of images from different subjects being classified as genuine is low. However, the chance of a pair of images from the same subject being classified as impostor is high. If t is low, we have the opposite scenario.

This matching measure takes advantage of the spatial relation between keypoints in a same image to penalize incorrect correspondences. Usually this idea is not used for 2D images due to the perspective distortion, which is only solved when the 3D information is available [20]. Since dermatoglyphic patterns are not affected by the perspective distortion, we can use the spatial information to estimate the similarity without having to find which correspondences are correct (Equation 5). Figure 6 illustrates this process, showing that the distance between keypoints is similar in images from the same subject (colored lines in Figures 6(a) and 6(b)) and different in images from other subjects (see Figure 6(c)).

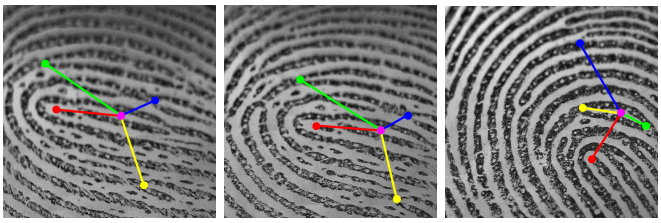

(a) (b) (c)

Fig. 6. Example of the spatial relation between keypoints.

A. Hierarchical matching

When an image is properly normalized for both location and orientation, it is possible to divide it in subregions and then individually apply the matching for each subregion. By doing so, it is possible to improve the recognition results if some regions of the image are damaged.

In this matching scenario, we have multiple score values s^1_{AB}, s^2_{AB}, ... and s^K_{AB}, where s^i_{AB} is the score value for the i-th subregion and K is the number of subregions. Then, we will have a threshold value t_i for each score s^i_{AB}, and also threshold values for each possible combination of two or more subregions by the sum rule [21] (*e.g.* t_{i+j} is the threshold for sum of the scores s^i_{AB} and s^j_{AB}). These thresholds are hierarchically applied, as in [22], to reduce the matching time and increase the accuracy as well. Figure 7 illustrates the hierarchical matching process. Even if all individual scores are below their respective thresholds, a matching between images from the same subject can still be correctly identified by the sum of scores. This is possible because, most of the time, the threshold for a sum of scores is lower than the sum of the thresholds for these scores (*e.g.* $t_{i+j} < t_i + t_j$).

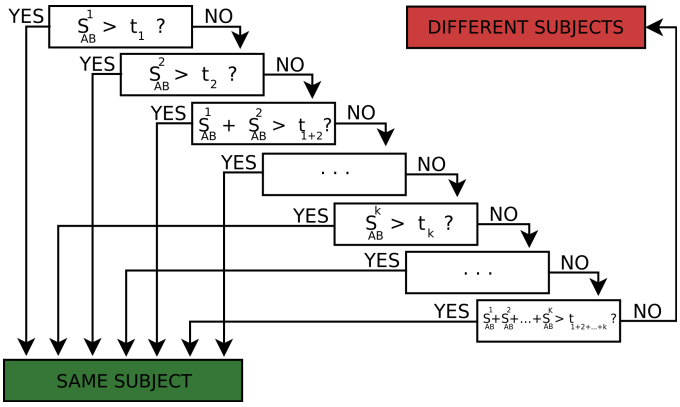

Fig. 7. Hierarchical matching of different subregions of a pair of images.

In this work, we horizontally divide palmprint and footprint images in four subregions because there are four interdigital regions in palmprints and footprints [23]. This way, we avoid errors in the correspondence determination caused by similar interdigital structures, such as core and delta points.

IV. Experimental results

We collected two different newborn image databases. To the best of our knowledge, there are no publicly available databases for newborn authentication. The first one, named NB_ID, was acquired by a 1000 ppi scanner (CrossMatch LSCAN[2]), and has 1221 palmprint and 1221 footprint images. The second one, named NB_ID_II, was acquired by a 2400 ppi sensor we developed for this work, and has 519 palmprint and 519 footprint images of 173 newborns. There are three palmprint and three footprint images for each newborn, and the images were collected no later than 48 hours after birth.

These images were automatically classified according to their quality in five levels as presented in [24]: good, normal, dry, wet and spoiled. We used the classification results to eliminate subjects that do not have enough quality images to be used in the recognition experiments. In NB_ID, only good and normal images are proper for recognition due to the low resolution. In our previous work [1], palmprint images from only 20 newborns with good images were selected for the recognition experiments (*i.e.* 60 images in total), which we will call subset NB_ID_A. We have extended this subset to include palmprints and footprints from 80 newborns (*i.e.* 240 images in total), called subset NB_ID_B.

In NB_ID_II, good, normal and dry images could be used for recognition since we have a higher resolution. In total, 297 palmprints and 231 footprints from 99 and 77 newborns, respectively, were selected for the recognition experiments, called subset NB_ID_II_B.

A. Pore detection results

In this experiment, we randomly cut a 100×100 region from 10 randomly chosen images from each newborn dataset (NB_ID_A, NB_ID_B and NB_ID_II_B). Then, we manually marked all pores in these cuts to compute the detection rate

[2]http://www.crossmatch.com/

and false discovery rate (FDR) values. On average, we detected 81% of the pores in newborn images (2400ppi) and obtained a 14.4% FDR. These results are comparable to the state-of-the-art results for adult fingerprint images with 1200ppi [8].

We do not reconstruct ridges or estimate ridge orientation and frequency to perform the detection, making the pore detection less expensive and also avoiding computing information that is not going to be used later for matching. These results also show the potential of the presented method regarding adaptability, since we have used newborn images with different resolutions and also adult images.

As may be seen, for a maximum displacement value between 5 and 10 pixels, the method perform well for all databases, obtaining results that are comparable to the state-of-the-art works in pore detection [8].

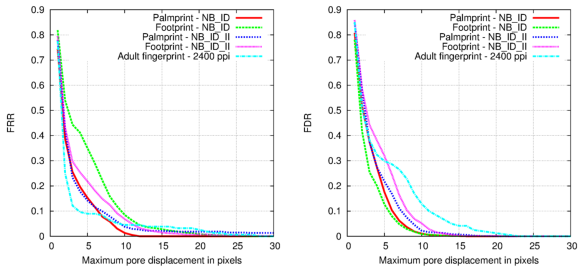

(a) (b)

Fig. 8. Pore detection results: (a) FRR and (a) FDR.

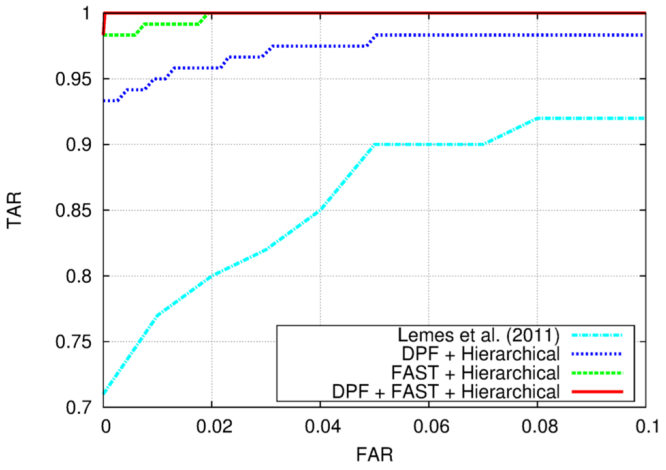

Fig. 9. Recognition comparison between our previous work and the proposed method.

B. Newborn authentication results

In our first experiment, we have compared the proposed matching method to our previous work [1] using NB_ID_A. Figure 9 shows this comparison, and, as may be seen, our new matching outperforms our previous results. The true acceptance rate (TAR) reaches 98% with a 0% false acceptance rate (FAR), while we achieve 71% in [1] with the same FAR. We also show that our hierarchical approach can be extended to combine both FAST and DPF keypoints to obtain more accurate results. We noticed that, when recognizing dermatoglyphic patterns through keypoints, the discrimination power of pores is complementary to corners, which are a keypoint widely used in the literature.

We performed a second experiment in order to evaluate the performance of the presented method across common acquisition problems. In this experiment, we used larger subsets (*i.e.* NB_ID_B and NB_ID_II_B) with images that have lower quality than the once in subset NB_ID_A. The results, presented in Figure 10, show that similar recognition rates are obtained for palmprint and footprint images. Also, the combination of FAST and DPF increases the recognition results. As may also be observed, the resolution plays a major role in the recognition task. For the subset NB_ID_II_B, even using dry images which are not as good as the images in subset NB_ID_B, we achieved about 94% TAR with 0% FAR, while we obtained only 86% TAR with 0% FAR for the subset NB_ID_B. These results corroborate the analysis presented by Weingaertner *et al.* [25], which concludes that at least 1500 ppi are necessary to perform newborn recognition with palmprints and footprints.

V. Conclusion

We have presented a novel method for newborn authentication by matching keypoints in a hierarchical framework. To this end, we have designed a novel pore detection method to extract keypoints from dermatoglyphic patterns.

Our pore detection results are comparable to the state-of-the-art, but our method does not require ridge reconstruction or ridge orientation and frequency estimation steps to do so. Therefore, our pore detector requires less computational resources than other methods in the literature.

For authentication, we show that is possible to reach 91.53% TAR for palmprints and 93.72% TAR for footprints with 0% FAR when high resolution images are available. Also, we considerably outperformed our previous work, achieving 98% TAR with 0% FAR in the subset of images with good quality, against 71% TAR obtained before. As a future work, we intend to investigate a multimodal approach using both palmprints and footprints to increase the recognition accuracy.

Acknowledgment

The authors would like to thank the financial support from the Federal University of Paraná and from the following funding agencies: Conselho Nacional de Desenvolvimento Científico e Tecnológico (CNPq) and Coordenação de Aperfeiçoamento de Pessoal de Nível Superior (CAPES).

References

[1] R. P. Lemes, O. R. P. Bellon, L. Silva, and A. K. Jain, "Biometric recognition of newborns: Identification using palmprints," in *International Joint Conference on Biometrics*, 2011, pp. 1–6.

[2] S. Bharadwaj, H. S. Bhatt, R. Singh, M. Vatsa, and S. K. Singh, "Face recognition for newborns: A preliminary study." in *Biometrics: Theory, Applications and Systems*, 2010, pp. 1–6.

[3] W. Jia, H. Cai, J. Gui, R. Hu, Y. Lei, and X. Wang, "Newborn footprint recognition using orientation feature." *Neural Computing and Applications*, pp. 1–9, 2010.

[4] S. Tiwari, A. Singh, and S. Singh, "Fusion of ear and soft-biometrics for recognition of newborn." *Signal and Image Processing: An International Journal*, vol. 3, no. 3, pp. 103–116, 2012.

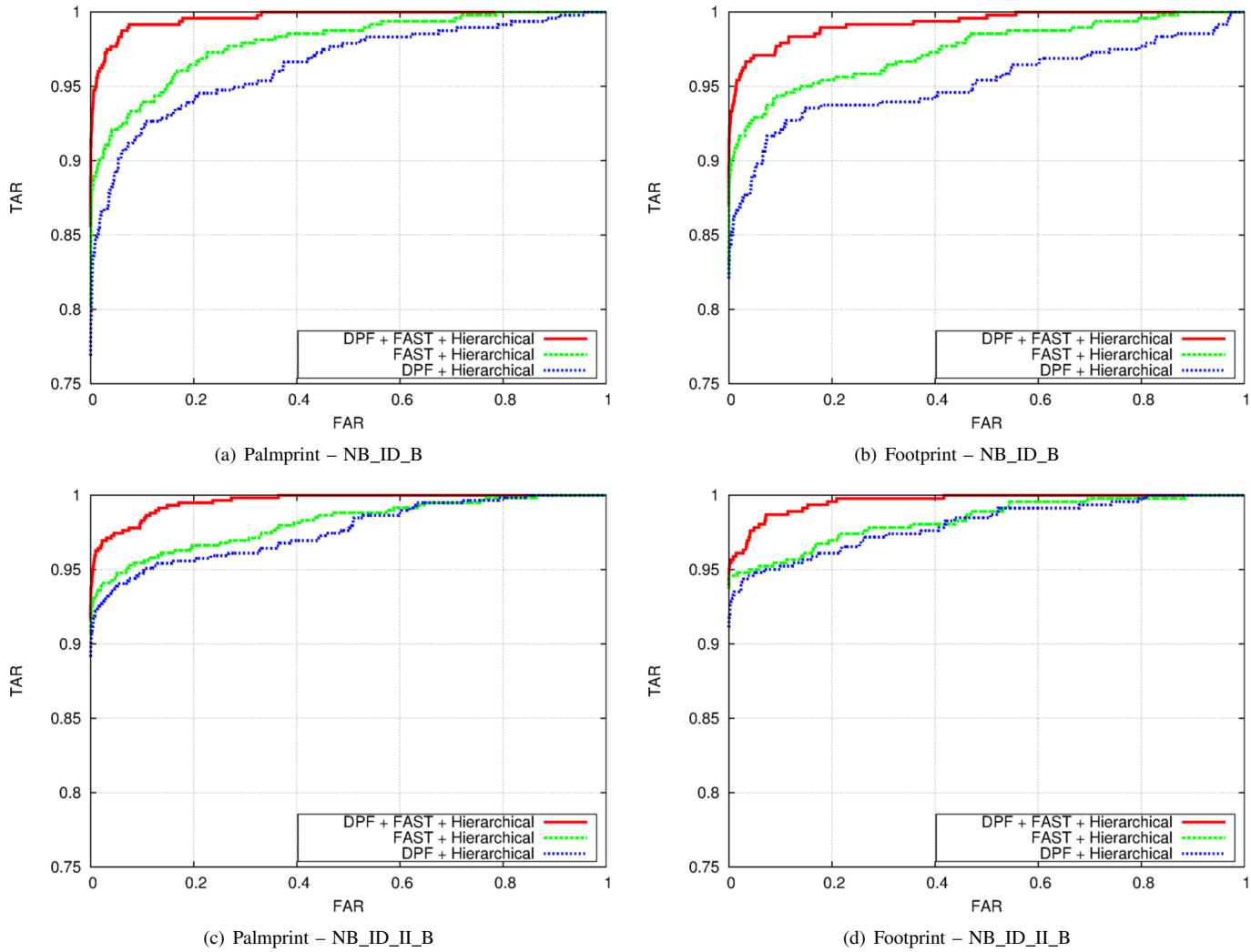

(a) Palmprint – NB_ID_B

(b) Footprint – NB_ID_B

(c) Palmprint – NB_ID_II_B

(d) Footprint – NB_ID_II_B

Fig. 10. Recognition results for different subsets.

[5] ——, "Intelligent method for face recognition of intant." *International Journal of Computer Applications*, vol. 52, no. 4, pp. 46–50, 2012.

[6] E. Rosten and T. Drummond, "Machine learning for high-speed corner detection," in *European Conference on Computer Vision*, ser. Lecture Notes in Computer Science. Springer Berlin Heidelberg, 2006, vol. 3951, pp. 430–443.

[7] A. K. Jain, C. Yi, and M. Demirkus, "Pores and ridges: High-resolution fingerprint matching using level 3 features," *IEEE Transactions on Pattern Analysis and Machine Intelligence*, vol. 29, no. 1, pp. 15–27, 2007.

[8] Q. Zhao, D. Zhang, L. Zhang, and N. Luo, "Adaptive fingerprint pore modeling and extraction," *Pattern Recognition*, vol. 43, no. 8, pp. 2833–2844, 2010.

[9] J. Chen and Y.-S. Moon, "Using sift features in palmprint authentication," in *International Conference on Pattern Recognition*, 2008, pp. 1–4.

[10] X. Shuai, C. Zhang, and P. Hao, "Fingerprint indexing based on composite set of reduced sift features," in *International Conference on Pattern Recognition*, 2008, pp. 1–4.

[11] S. Klein and D. Murray, "Parallel tracking and mapping for small AR workspaces," in *Proc. Sixth IEEE and ACM International Symposium on Mixed and Augmented Reality*, Nara, Japan, November 2007.

[12] L. Silva, O. R. P. Bellon, R. Lemes, J. Meira, and M. N. L. Cat, "An image processing tool to support gestational age determination," in *Int'l Symposium on Computer-Based Medical Systems*, 2006, pp. 867–874.

[13] S. M. Pizer, R. E. Johnston, J. P. Ericksen, B. C. Yankaskas, and K. E. Muller, "Contrast-limited adaptive histogram equalization: speed and effectiveness," in *Conf. Visualization in Biomedical Computing*, 1990, pp. 337–345.

[14] N. Otsu, "A threshold selection method from gray-level histograms," *Transactions on Systems, Man, and Cybernetics*, vol. 9, no. 1, pp. 62–66, 1979.

[15] P. Viola and M. Jones, "Rapid object detection using a boosted cascade of simple features," in *Computer Vision and Pattern Recognition*, vol. 1, 2001, pp. I–511–I–518.

[16] E. Tola, V. Lepetit, and P. Fua, "Daisy: An efficient dense descriptor applied to wide-baseline stereo," *IEEE Transactions on Pattern Analysis and Machine Intelligence*, vol. 32, no. 5, pp. 815–830, 2010.

[17] D. G. Lowe, "Object recognition from local scale-invariant features," in *International Conference on Computer Vision*, vol. 2, 1999, pp. 1150–1157.

[18] H. Bay, A. Ess, T. Tuytelaars, and L. Van Gool, "Speeded-up robust features (surf)," *Computer Vision and Image Understanding*, vol. 110, no. 3, pp. 346–359, 2008.

[19] J. L. Bentley, "Multidimensional binary search trees used for associative searching," *Communications of the ACM*, vol. 18, no. 9, pp. 509–517, 1975.

[20] M. Pamplona Segundo, L. Gomes, O. R. P. Bellon, and L. Silva, "Automating 3d reconstruction pipeline by surf-based alignment," in *International Conference on Image Processing*, 2012, pp. 1761–1764.

[21] J. Kittler, M. Hatef, R. P. W. Duin, and J. Matas, "On combining classifiers," *IEEE Transactions on Pattern Analysis and Machine Intelligence*, vol. 20, no. 3, pp. 226–239, 1998.

[22] C. C. Queirolo, L. Silva, O. R. P. Bellon, and M. Pamplona Segundo, "3D face recognition using simulated annealing and the surface interpenetration measure," *IEEE Transactions on Pattern Analysis and Machine Intelligence*, vol. 32, no. 2, pp. 206–219, 2010.

[23] H. Cummins and M. Midlo, *Finger Prints, Palms and Soles: An Introduction to Dermatoglyphics*. Dover Publications, 1961.

[24] C. Wu, S. Tulyakov, and V. Govindaraju, "Image quality measures for fingerprint image enhancement," in *Int'l Conf. Multimedia Content Representation, Classification and Security*, 2006, pp. 215–222.

[25] D. Weingaertner, O. R. P. Bellon, M. N. L. Cat, and L. Silva, "Newborn's biometric identification: can it be done?" in *International Conference on Computer Vision Theory and Applications*, 2008, pp. 200–205.